ABSTRACT

Title of Thesis:	REVOLUTIONARY FLIGHT VEHICLE BASED ON LEONARDO DA VINCI AERIAL SCREW: A PARADIGM SHIFT IN VTOL TECHNOLOGY
	Austin Christopher Prete, Master of Science, 2022
Thesis Directed By:	Alfred Gessow Professor and Director, Dr. Inderjit Chopra, Aerospace Engineering

Aerial screws are rotors that consist of continuous large solidity single surface blades, which are able to provide significant thrust and control authority at increased power consumption when compared to traditional rotor blades. By leveraging a unique bound tip vortex, also observed in delta-wings, aerial screws are able to attain figure of merit values nearing 0.7 or higher, comparable to a modern rotorcraft. To prove the function of aerial screws, physical models were fabricated and flight tested. The primary objective of this paper is to explore the performance of a 6-in (0.152 m) diameter aerial screw and compare its performance with a 6-in (0.152 m) diameter traditional rotor, to demonstrate its feasibility in a quadrotor configuration and to show its efficiency as determined in the student designs from the 2019-2020 VFS student design competition.

REVOLUTIONARY FLIGHT VEHICLE BASED ON LEONARDO DA VINCI AERIAL SCREW: A PARADIGM SHIFT IN VTOL TECHNOLOGY

by

Austin Christopher Prete

Thesis submitted to the Faculty of the Graduate School of the
University of Maryland, College Park, in partial fulfillment
of the requirements for the degree of
Master of Science
2022

Advisory Committee:
Professor Inderjit Chopra, Chair
Dr. Anubhav Datta
Dr. James Baeder

Dedication

To my family for their unwavering support throughout my entire life.

Acknowledgements

I would like to thank my advisors Dr. Inderjit Chopra and Dr. Vengalattore Nagaraj for providing continued guidance and support while working through multiple projects and tough times. Their dedication to their students is awe inspiring.

I would also like to thank Dr. Anubhav Datta for his incredible support as a professor during the most strenuous semesters of my life.

I am also thankful to my classmates turned friends for their support. Ehis for all his help during late nights in the cube farm, Ilya for being an always forward marching friend and Robert for his extensive patience and urgency at the same time. Lastly, but not least, Peter for his effort and interest in publicizing the aerial screw in the outside world. Thanks in part to his investment, the Aerial screw has been published in articles worldwide.

Of course, this research would not have been possible without the tremendous effort of the UMD 2020 Helicopter Graduate Design team. To them I am ever thankful for their effort in producing an extensive database of knowledge and experiments from which this project was born. I hope seeing a flying version of the concept you spent months losing sleep over is as satisfying for you as it is for me.

As with nearly every acknowledgement section, I will have inadvertently missed including several people vital to the completion of this project and the corresponding degree. To them I am again thankful for their support.

Table of Contents

DEDICATION II
ACKNOWLEDGEMENTS III
TABLE OF CONTENTS IV
LIST OF TABLES V
LIST OF FIGURES VI
CHAPTER 1: INTRODUCTION, HISTORY & MOTIVATION OF AERIAL SCREW VEHICLES 1
  Introduction 1
  History of Aerial Screws 3
  Modern Designs of Aerial Screws 5
CHAPTER 2: GEOMETRY OF AN AERIAL SCREW 7
  Continuous Surface Geometry Features 7
    Leading and Trailing Edge 8
    Anhedral and Dihedral 8
    Swept Tip Section 9
CHAPTER 3: UNIQUE AERODYNAMICS OF AERIAL SCREWS 10
  Bound Tip Vortex of Aerial Screws 10
    Delta-wing Airplane Analogues 11
    CFD Analysis of UMD Designs 11
CHAPTER 4: DESIGN OF 15.25 CM (6-IN) DIAMETER AERIAL SCREW 13
  Initial Physical Rotor Parameters 13
  Material Selection 14
  Flattening Geometry of Aerial Screws 15
CHAPTER 5: FABRICATION OF 15.25 CM (6-IN) DIAMETER AERIAL SCREWS 17
  Initial Physical Rotor Parameters 17
  Methods of Machining and Motor Mating 18
  Initial Results of Early Fabrication 20
  Updated Rotor Fabrication 21
CHAPTER 6: TESTING A FUNCTIONAL AERIAL SCREW VEHICLE 23
  Stabilization of the Vehicle 23
  Stabilization of the Vehicle 25
    Control Scheme 25
  Flight Testing 27
    Hover 27
    Forward Flight 30
CHAPTER 7: DISCUSSION OF RESULTS 32
  Discussion 32
  Future Considerations 33
  Conclusions 33
BIBLIOGRAPHY 34

List of Tables

Table 1. Geometric parameters of first-generation physical aerial screw. 17
Table 2: Mass of each rotor part with different shafts. 20
Table 3: Aerial screw and traditional rotor generalized rotor performance................ 28

List of Figures

Figure 1: Leonardo DaVinci's concept aerial screw vehicle from Manuscript B, Folio 83V.......... 1
Figure 2: Full quadrotor vehicle with aerial screws in final configuration.......... 2
Figure 3: Full quadrotor vehicle with aerial screws airborne during indoor test.......... 2
Figure 4: Enrico Forlani's 1877 concept rotorcraft utilizing spar and blade geometry similar to aerial screws.......... 3
Figure 5: Paul Cornu's 1907 rotorcraft utilizing large solidity counter-rotating rotor blades. 4
Figure 6: The Technical University of Delft undergraduate team's aerial screw rotorcraft design utilizing single-blade ducted rotors. 5
Figure 7: The University of Maryland graduate team's rotorcraft design utilizing 4 open-air single-blade aerial screws. 6
Figure 8: Illustration of basic variable aerial screw geometry components. 7
Figure 9: An Archimedes Windmill utilizing 3 blades, variable dihedral, radius and pitch.......... 8
Figure 10: Computational Fluid Dynamics (CFD) model illustrating the low-pressure tip vortex through local vorticity. 10
Figure 11: Tip vortex formation of delta-wing fixed-wing aircraft at high angle of attack.[3].......... 11
Figure 12: Final CAD model for use in fabricating physical aerial screws. 13
Figure 13: The first iteration of aerial screw with wooden shaft without upper surface. 14
Figure 14: Outer and inner radial curves of 3D surface geometry for aerial screws. . 15
Figure 15: Flattened aerial screw surface material elements with curved leading and trailing edge. 16
Figure 16: Oversized skin material templates for measuring mylar surface. 18
Figure 17: Attempted mating methods for aerial screw shafts. Helicoil and threaded inserts left, 3D printed adapter right. 19
Figure 18: "6x4.5" quadcopter rotor blades used for comparison to aerial screws. ... 20
Figure 19: Current 2-bladed, single turn, novel Leonardo da Vinci aerial screw rotor. 21
Figure 20: Aluminum shaft closeup of internal threads and exterior spar through-holes. 22
Figure 21: Plot of aerial screw and traditional rotor thrust as a function of electrical power.......... 23
Figure 22: Plot of aerial screw and traditional rotor thrust as a function of RPM...... 24

Figure 23: Plot of aerial screw and traditional rotor FM as a function of RPM. 24
Figure 24: Plot of aerial screw and traditional rotor Coefficient of Thrust as a function of FM. 24
Figure 25: Performance test values of aerial screws and traditional rotors. 28
Figure 26: Plot of different VTOL vehicle configuration's power loading vs. disk loading. 29
Figure 27: Plot of different mini-VTOL vehicle configuration's power loading vs. disk loading. 30
Figure 28: Traditional rotor forward flight power curve using frame and hardware of aerial screw vehicle. 31
Figure 29: Aerial screw forward flight power curve. 31

Chapter 1: Introduction, History & Motivation of Aerial Screw Vehicles

Introduction

Aerial screws have long been envisaged for vertical flight, with the first aerial screw conceived by Leonardo da Vinci, seen in Figure 1, in the 1500s, while a later attempt at fabricating a large solidity helicopter occurred in the late 1800s.[1] Ultimately, the aerial screw was overtaken by a conventional rotor consisting of large aspect ratio, low solidity, airfoil blades in the realm of vertical flight due to their proven performance. This study serves to introduce a working physical model of an aerial-screw-based vehicle iterated from Leonardo da Vinci's concept of over 500 years ago, demonstrating the flight potential of aerial screws.

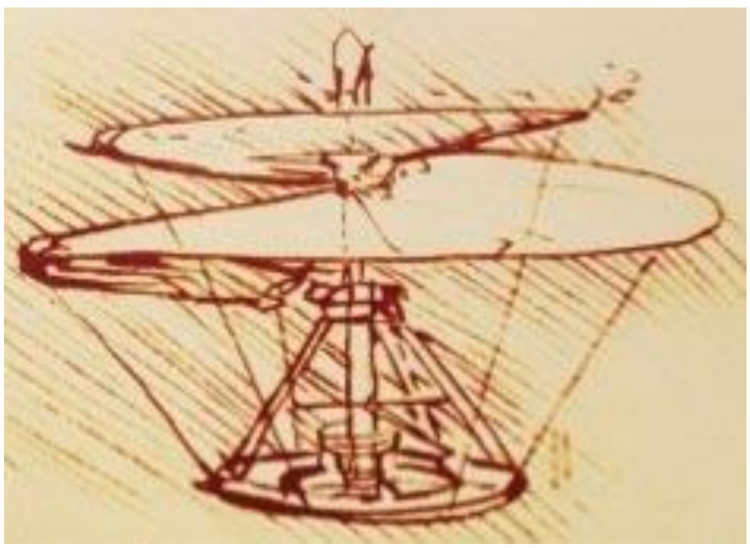

Figure 1: Leonardo DaVinci's concept aerial screw vehicle from Manuscript B, Folio 83V.

To demonstrate the concept, a quadrotor using four 3-inch radius aerial screws was developed, as shown in Figures 2 and 3, and flight-tested to show the capabilities of this vehicle and to compare its performance to a traditional rotor of the same diameter.

Figure 2: Full quadrotor vehicle with aerial screws in final configuration.

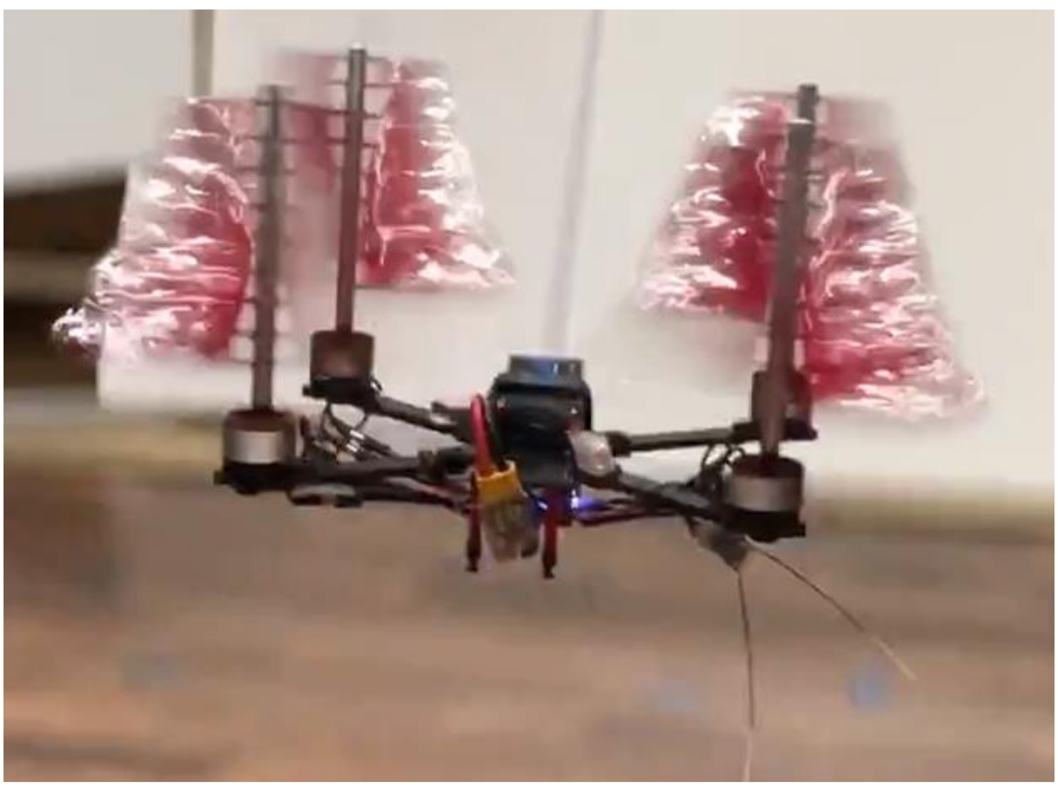

Figure 3: Full quadrotor vehicle with aerial screws airborne during indoor test.

Aerial screws maintain a unique geometry compared with traditional rotors, where their elongated "tip" region provides the ability to generate the unique lifting mechanism of a tip vortex. The first-place winner in the 2020 Vertical Flight Society (VFS) graduate student design competition, the University of Maryland (UMD), designed computer models of aerial screws that determined the primary lifting mechanism to be a continuous tip vortex.[2] It should be noted that the author of this paper was a member of the winning graduate student design team. Interestingly, the aerial screw tip vortex has functional similarities to delta-wing aircraft leading edge vortices,[3] lending itself the opportunity to have its flight mechanics explained via existing methods.

History of Aerial Screws

In the 1500s, Leonardo da Vinci envisioned the first aerial screw in one of his works titled Manuscript B Folio 83v. The conceptual functionality lay in the screw's ability to displace a large quantity of air relative to the surface area of the screw. Issues presented themselves in the form of powerplant choice, effective RPM, anti-torque capability and practical thrust to weight ratio. Despite the concept being incapable of flight by itself, other forms of vertical takeoff and landing (VTOL) vehicles were conceived from this initial inspiration.

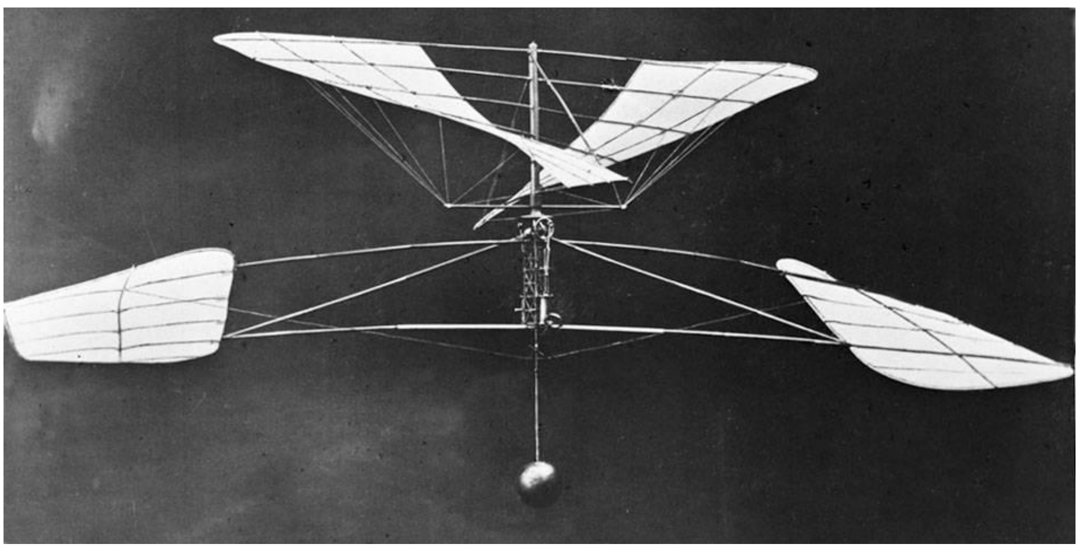

Figure 4: Enrico Forlani's 1877 concept rotorcraft utilizing spar and blade geometry similar to aerial screws.

A few large solidity helicopters were attempted as concepts in the 1800s. One such concept by Enrico Forlani, seen in Figure 4, includes two pairs of counter-rotating spiral shaped blades. Also in the 1800s, Paul Cornu designed and built a full-scale helicopter with short radius, high solidity, flat-plate rotors seen in Figure 5. Cornu's design managed to achieve short hops up to 5 meters leveraging the yet unknown ground effect. Unlike Leonardo's design, both designs managed to overcome the issue of anti-torque imbalance present in all helicopters/VTOL vehicles by incorporating secondary rotors spinning in the opposite direction of the first rotor. A special point of interest is the spar layout and progression used in the Forlani design, as it is fabricated such that it has some parallelism to that of DaVinci's aerial screw vehicle. Forlani's design utilized linear spars that passed through the central shaft creating a screw shaped aerial surface, albeit with lower solidity. Some other designs also shared several key aspects of the original aerial screw.

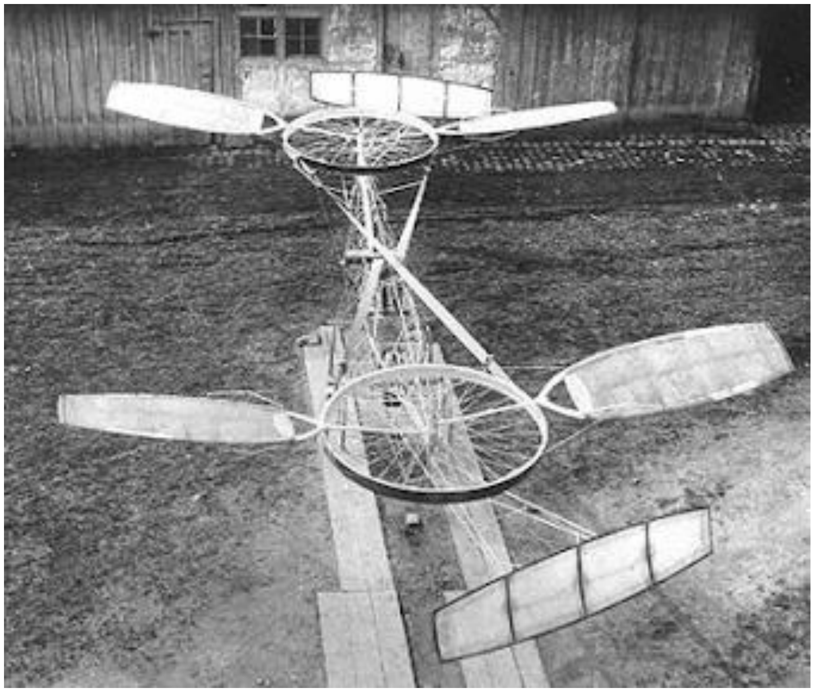

Figure 5: Paul Cornu's 1907 rotorcraft utilizing large solidity counter-rotating rotor blades.

Helicopter Blade Design: Despite initial concepts of VTOL vehicles being those of large solidity, the prevailing helicopters consisting of large aspect ratio, low solidity blades overtook the aerial screws due to their proven performance. The main differences of helicopter blades to aerial screw surfaces present themselves in the form of airfoils and low solidity. Traditional rotor blades consist of low solidity and high aspect ratio. Due to the large aspect ratio, a large mass of air with low induced velocity is achieved. As a result of the low induced velocity, thrust to sustain weight is achieved with minimum induced power.

Traditional rotorcraft blades have managed to achieve high figure of merit (FM) values greater than 0.7 where FM is defined as,

$$FM = \frac{Ideal\ Power}{Actual\ Power}$$

indicating that a high hover efficiency for traditional rotor blades has been established. Aerial screws can be characterized in the same fashion for the generated thrust using general momentum theory relations. Testing has shown that the aerial screws also follow the predicted values of thrust from momentum theory regardless of having a geometry unlike traditional rotorcraft.

Modern Designs of Aerial Screws

In 2020, the VFS student design competition sponsored by Leonardo Helicopters Company tasked multiple universities with the design and analysis of a functional aerial screw vehicle. Graduate and undergraduate teams from several universities designed multiple configurations of aerial screws capable of meeting key performance metrics such as FM, disk loading (DL), etc. Two standout first-place designs of aerial screws include the undergraduate and graduate teams respectively from Delft University of Technology and the University of Maryland.

Figure 6: The Technical University of Delft undergraduate team's aerial screw rotorcraft design utilizing single-blade ducted rotors.

The Delft undergraduate team designed a ducted aerial screw, seen in Figure 6, which leverages the aerial screw's continuous surface to displace large quantities of air similarly to DaVinci's design. The screw blade leverages a single varying pitch surface with elongated airfoil sections over the 360° swept surface. From Blade Element Theory (BET) analysis, commonly used for traditional rotorcraft, the team found a single 2ft radius rotor spinning at 1500 RPM was capable of producing a significant FM of 0.68; a performance metric rivaling some modern rotorcraft designs.

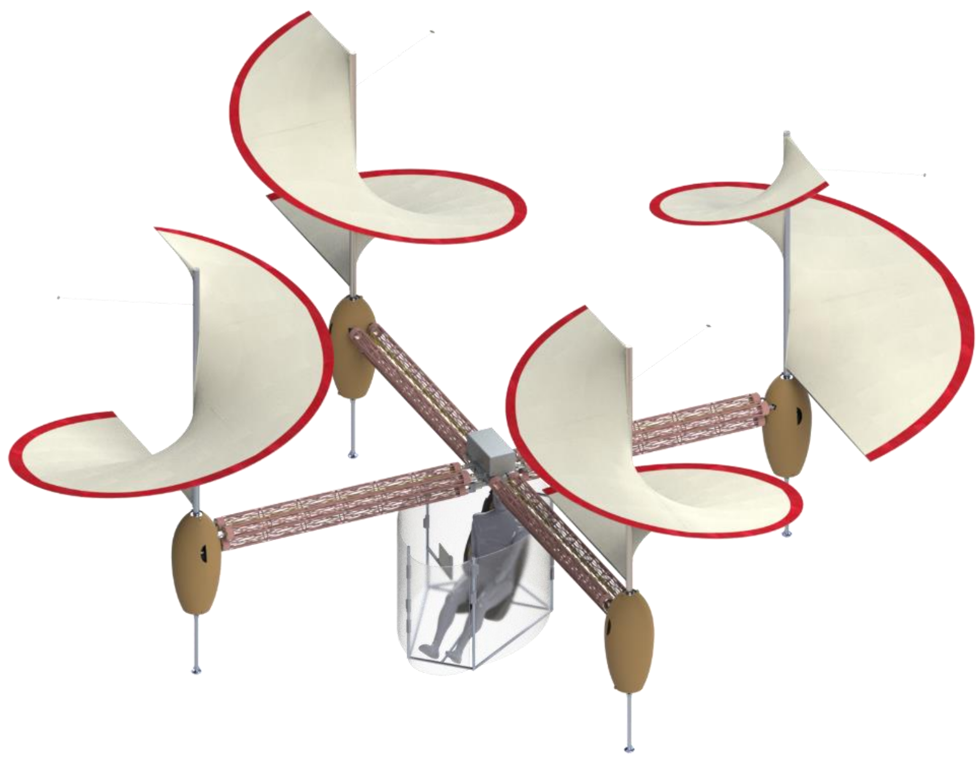

Figure 7: The University of Maryland graduate team's rotorcraft design utilizing 4 open-air single-blade aerial screws.

The graduate team from the University of Maryland designed an unenclosed aerial screw vehicle leveraging flight mechanics unique to aerial screws. Figure 7 shows the graduate design which includes four single-bladed rotors spinning at 367 RPM and producing a significant FM of 0.35 in hover. Physical testing of smaller scale open-air rotors in slightly more complex configurations had yielded FM values in the 0.65 to 0.7 range, again rivaling modern rotorcraft. The best efficiency design tested in the small scale by the UMD team was that of a dual blade tapered aerial screw utilizing the ratios of the full-scale design. Thus, this report utilizes similar geometric ratios for the final physical vehicle.

Chapter 2: Geometry of an Aerial Screw

Continuous Surface Geometry Features

Aerial screws derive their shape from a continuous surface similar to an Archimedes screw or mechanical screw. The shape of the single winding feature wrapped around a central shaft in a helical pattern determines the type of screw. A low screw radius to shaft radius ratio may determine a screw to be mechanical, and a large screw radius to shaft radius ratio leans toward an aerial screw. Typically, Archimedes screws are meant for transportation of liquids or solid particulate masses when in motion. Aerial screws inherently are meant to displace low density air rather than higher density solids and liquids, requiring less supporting material and lighter overall fabrication.

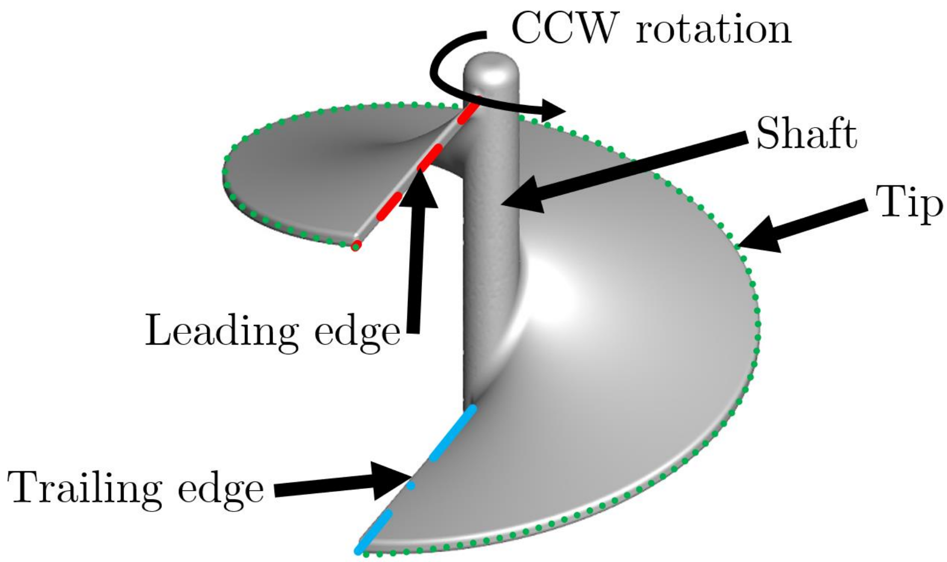

Figure 8: Illustration of basic variable aerial screw geometry components.

Figure 8 shows the basic variable geometry of an aerial screw. The defining features of an aerial screw are the number of revolutions per blade and pitch of the blades. Modern high aspect ratio blades use twist to determine local pitch, however aerial screws can define pitch between sections of blade that overlap with themselves. Local pitch of aerial screw sections used for aerodynamic element analysis are determined by the radius and height separation of blade sections. Due to the surface geometry of aerial screws, radial strips follow the "ideal twist" found in Leishman's *Principles of helicopter Aerodynamics*.[4] The surface follows a quadratic negative twist due to the elongated nature of the surface. As such, adjusting pitch or twist requires additional considerations.

Leading and Trailing Edge

Similar to modern rotorcraft blades, aerial screws have leading and trailing edges, but both play a less important role in the function of an aerial screw for the primary lifting mechanism. A blunt leading edge and sharp trailing edge may provide some benefit to the performance, but most likely will have less influence on the performance than observed with modern rotorcraft blade's leading and trailing edge adjustments. Because the effect of leading and trailing edge geometry is supposed minimal, it was not explored in this study as a means of improving performance at the scale tested.

Anhedral and Dihedral

Anhedral is another notable aspect of aerial screws that functions similarly to flap and pre-cone on normal rotor blades. Aerial screws developed in this paper cannot change their "flap" angle during operation, potentially limiting the efficiency of rotors in different flight regimes. Flap can both be upward (dihedral, positive coning) or downward (anhedral, negative coning), resulting in some performance changes. Certain turbine generator screws, such as *The Archimedes Windmill* seen in Figure 9, include dihedral to increase efficiency. By capturing axial air and preventing it from uncontrollably flowing laterally, the turbine is able to extract more energy from the air.

Figure 9: An Archimedes Windmill utilizing 3 blades, variable dihedral, radius and pitch.

The main difference between optimizing for a turbine and aerial screw is the requirement to convert as much wind energy to rotational energy in a turbine instead of transforming the rotational energy to axial force (thrust) in an aerial screw. Due to this swapping of energy direction, the dihedral would also swap directions, such that an aerial screw has an anhedral. Adding the anhedral would cause lateral flow to decrease in an aerial screw. As such, large anhedral angles are avoided in order to maintain the effect of the primary lifting mechanism for open-air aerial screws.

Swept Tip Section

Unlike most rotorcraft blades, the tip of an aerial screw is able to sweep along a range of radii creating a tapered side profile. By varying the radius at changing radial stations, aerial screws are able to follow and force the position of a bound tip vortex to increase thrust. The bound vortex, explained in more detail in the following section, provides most of the thrust for an aerial screw and thus determines the areas of most attention when designing an aerial screw.

Chapter 3: Unique Aerodynamics of Aerial Screws

Bound Tip Vortex of Aerial Screws

Modern rotorcraft depend on the lifting capabilities of airfoil geometry in high aspect ratio blades, utilizing differential pressure and redirection of air to generate thrust. Rotorcraft amplify and modify several aerodynamic features that are present in fixed wing aircraft such as large rotor downwash and contraction, tip vortex interactions with tail rotors, limited forward flight speed due to reverse flow regions, etc. Several of these differences are overcome with additions to helicopters making them compound rotorcraft, but aerial screws leverage unique aerodynamic aspects and lessen the influence of other detrimental elements such as downwash.

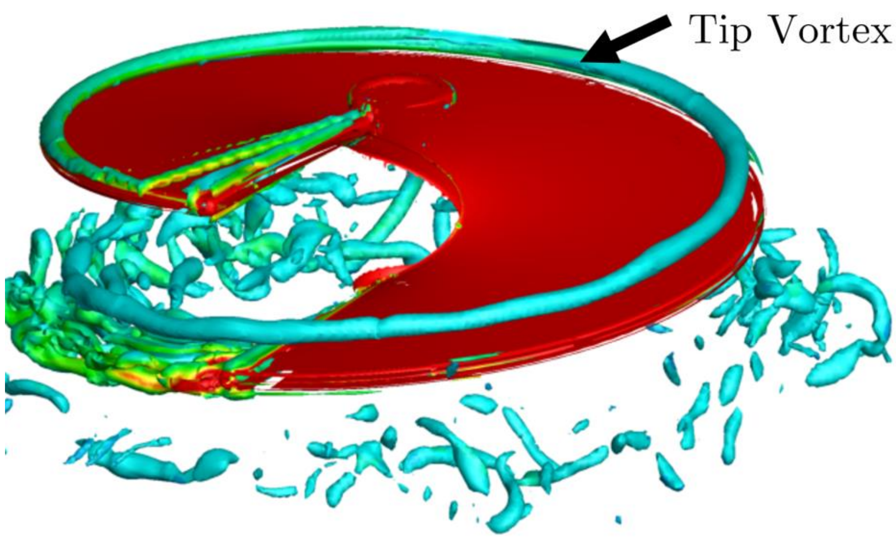

Figure 10: Computational Fluid Dynamics (CFD) model illustrating the low-pressure tip vortex through local vorticity.

As with other flight vehicles, aerial screws redirect air via the shape and pitch of the surface to generate thrust; however, aerial screws utilize a bound tip vortex, illustrated in Figure 10, to generate most of the vehicle lift. In fixed wing and rotary wing flight mechanics, a tip vortex serves to reduce the lift near the tip of the lifting surface due to equalizing pressure between the upper and lower surfaces. The tip vortex exists because of the difference of the higher-pressure underside to the lower-pressure upper surface. Because airfoils are not enclosed with sealed boundaries, excluding ducted airfoils, the pressure difference causes radial flow or lateral flow in rotorcraft and fixed wing aircraft respectively. The lateral flow from the higher-pressure region underneath the surface then proceeds to trend toward the lower pressure region above the surface, causing vortices about the tip.

Delta-wing Airplane Analogues

Aerial screws form a tip vortex just as other rotorcraft do, which lends itself to increase the pressure difference between the upper and lower surfaces similar to a delta-wing airplane. Figure 11 illustrates the perceived "tip vortex" (actually leading-edge) of a general delta-wing shaped surface. The leading-edge vortex of a delta-wing airplane has potential operational differences based on tip-geometry changes.[3] Likewise, the tip section of an aerial screw may be subject to differing flight characteristics and could be optimized via adjusting the tip region geometry.

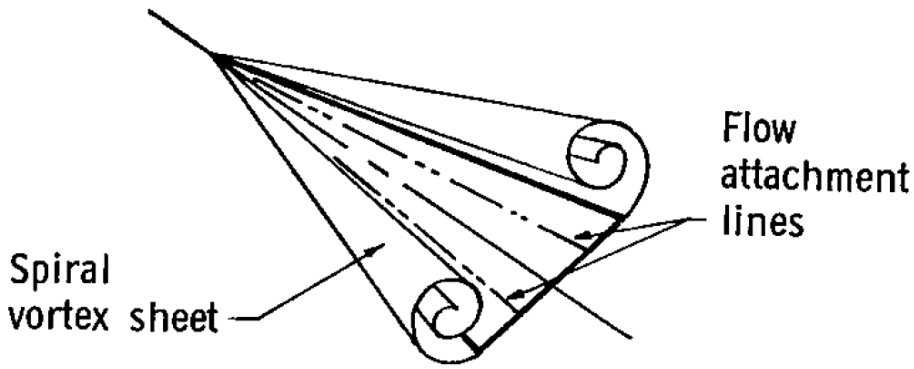

Figure 11: Tip vortex formation of delta-wing fixed-wing aircraft at high angle of attack.[3]

Delta-wing airplanes leverage high angle of attack flat plate surfaces to create high pressure underneath the wing where flow slows down. As the high-pressure air underneath the wing is forced around the leading edge/tip of a delta-wing, it curves into a bound leading-edge vortex which reduces pressure at the upper surface in the leading-edge region. This pressure difference accounts for nearly 80% of the lift of a delta-wing aircraft when in subsonic flight regimes. Similarly, aerial screws take advantage of the bound tip vortex to produce a significant percentage of lift. By displacing air underneath the blades, the tip section becomes the main region where lateral flow occurs, providing an opportunity for vortices to form.

CFD Analysis of UMD Designs

During the design phase of the 2020 VFS competition, the UMD graduate team conducted in-house CFD analysis to determine the interactions and lifting mechanisms for multiple aerial screw configurations. In each case, the pressure distribution revealed an area of low pressure near the tip region on the upper surface, indicating an unexpected aerodynamic mechanism at play. As mentioned earlier, the mechanism is a bound tip vortex, which functions similarly to fixed-wing delta-wing leading edge vortices. CFD results from the UMD graduate design team present nearly 80% of thrust of an aerial screw is generated by the bound tip vortex, indicating the region where it is formed and maintained being vital to the overall performance of the vehicle.[2]

Preliminary analysis also helped to determine improved geometries for the aerial screws. Differing pitch, radial taper and number of turns allow for best case scenarios to be identified. One of the top contenders identified was that of an aerial screw having a 2:1 taper ratio with 1 full revolution of a blade and approximately a 1.33:1 pitch to radius ratio. A more ideal configuration would include anhedral angle, but would not lend itself to easy repeatable construction for a technology demonstrator. As such, the final designs included no anhedral, sacrificing a small margin of performance for mechanical simplicity. Undergraduate testing of physical rotors at the university of Maryland revealed FM capabilities up to 0.7 or higher when including a second aerial screw blade on a single rotor, thus prompting the addition of a second blade to each newly fabricated rotor. Additionally, a second blade would reduce complexity when attempting to balance rotors.

Chapter 4: Design of 15.25 cm (6-in) Diameter Aerial Screw

Initial Physical Rotor Parameters

Aerial screw designs were initially conceived for large rotors capable of carrying a human payload, but alterations were required to suit a smaller test vehicle. Alterations in the form of material selection, mating methods and structural requirements were investigated. Material selection and mating methods proved to be the areas of most concern when designing the rotors.

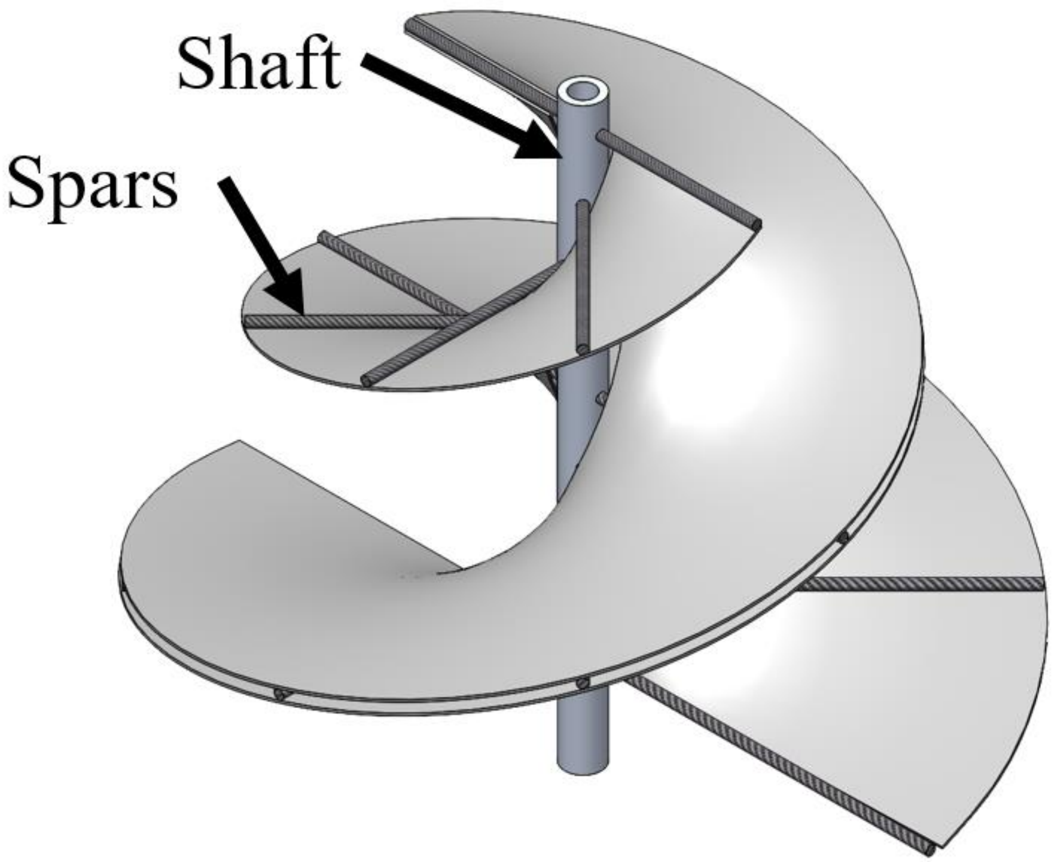

Figure 12: Final CAD model for use in fabricating physical aerial screws.

For the aerial screws tested in this report, the rotors were designed with simplistic spar placements and surface covering. Each carbon fiber spar was positioned equidistant from each other such that the top and bottom spars were separated from each other by 10.15 cm (4-in). The nine spars were offset by 45° from each other to obtain a full 360° sweep from leading edge to trailing edge. Figure 12 illustrates the spar layout of the novel aerial screw design with upper surface removed on one blade. Tip wire (not seen) was added along the profile of the tip section to maintain surface tension and to assist load transfer.

Material Selection

Materials of aerial screws were determined by ease of manufacturing/assembly and light weight. Initial designs of 6” diameter aerial screws prioritized weight reduction, since expected thrust would be much lower than traditional rotor blades. Preliminary testing of 3D printed 30mm diameter micro-quadcopter blades proved far too heavy, being over 8 times heavier than standard injection molded rotor blades. As such, the vehicle was incapable of hover even in ground effect. Thrust testing of the micro-scale rotors showed a reduction in thrust of 30% compared to the injection molded blades. The increased weight combined with decreased thrust incentivized reducing the weight of larger scale aerial screws over refining screw geometry or fabrication techniques.

Figure 13: The first iteration of aerial screw with wooden shaft without upper surface.

The first iteration of aerial screw seen in Figure 13 was designed with 1.25cm (0.5in) diameter wooden shaft with nine protruding carbon fiber rods, two steel tip wires (one for each blade per rotor) and 2 lower surfaces comprised of lightweight hobby mylar. The main shaft included the possibility of solid metal replacements, but were deemed unsuitable due to a predicted weight more than twice that of a structurally equivalent

wooden shaft. Carbon fiber was chosen as the spar material due to the weight reduction over a comparable metal spar and the reduced spatial requirement compared to a wooden spar. Steel tip wire was chosen as it fit the requirements of a semi-stiff surface tensioning material that could be shaped into a thin tapered spiral. Custom laid carbon fiber tow would produce the same effect, but would also increase cost and fabrication complexity, potentially reducing consistency between rotors. If custom molds were fabricated for tip carbon fiber strings, tip consistency would increase while allowing for identification and testing of various tip geometry. Due to cost and time constraints, carbon fiber tip sections were not explored.
The surface material of larger scale aerial screws designed in the 2020 VFS competition included carbon fiber layups, metal sheeting and sail cloth. Each of those materials when scaled down would provide too much weight in a relatively low load scenario. Thus, a less dense, low strength material of hobby grade mylar was chosen. The ability to conform to non-linear shapes would prove invaluable during construction, as the geometry of an aerial screw surface is unable to be flatly unwrapped nor converted to an unstretched 2D shape.

Flattening Geometry of Aerial Screws

The finalized aerial screw surface geometry included an inner radius of 0.635cm (0.25in) and maximum outer radius of 7.62cm (3in), meaning the local pitch value changed from nearly 60° to 15° along the chord, mimicking the ideal quadratic twist of a modern helicopter blade. Unfortunately, due to the rotor's long swept blade chord seen in Figure 14, the required inner material length was found to be 10.7cm (4.2in) while the outer material length was found to be 37.5cm (14.75in). This presented a problem if trying to fabricate the surface from a 2D material, as a simple flattened geometry with 0.635cm (0.25in) radius interior would be required to stretch over 3 times its own circumference to fit the aerial screw curve.

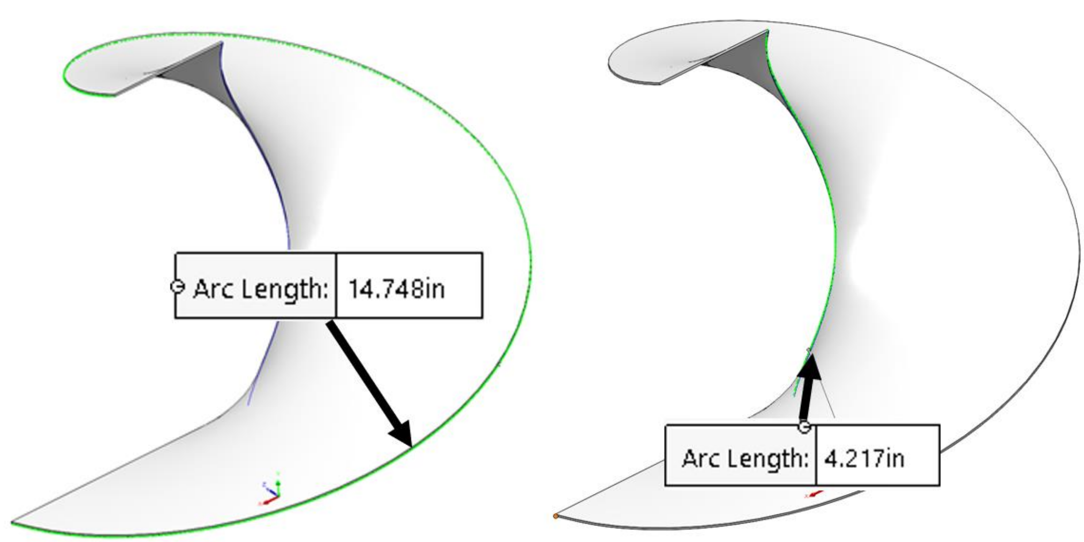

Figure 14: Outer and inner radial curves of 3D surface geometry for aerial screws.

The surface of an aerial screw cannot be made from a single continuous section of non-stretchable flat material. Take the example of the outer surface of a cone which can be flattened out in the shape of a semicircle with the center derived from the tip of the cone. The shape is able to be flattened due to the center of the “circle” being located at the same vertical position in the cone regardless of radial station. An aerial screw includes vertical displacement alongside a sweeping “circular” surface, removing the possibility of a single flattened surface. The design of variable anhedral screw surfaces can be flattened into a single surface, since the anhedral changes to match the vertical displacement at each radial station. Because the anhedral remains constant for current aerial screw designs (for ease of fabrication and consistency), the aerial screw surface cannot be flattened into a single non-stretchable surface. The surface is capable of being split into smaller segments, however consistency between rotors would suffer without reducing the overall amount of material warping necessary.

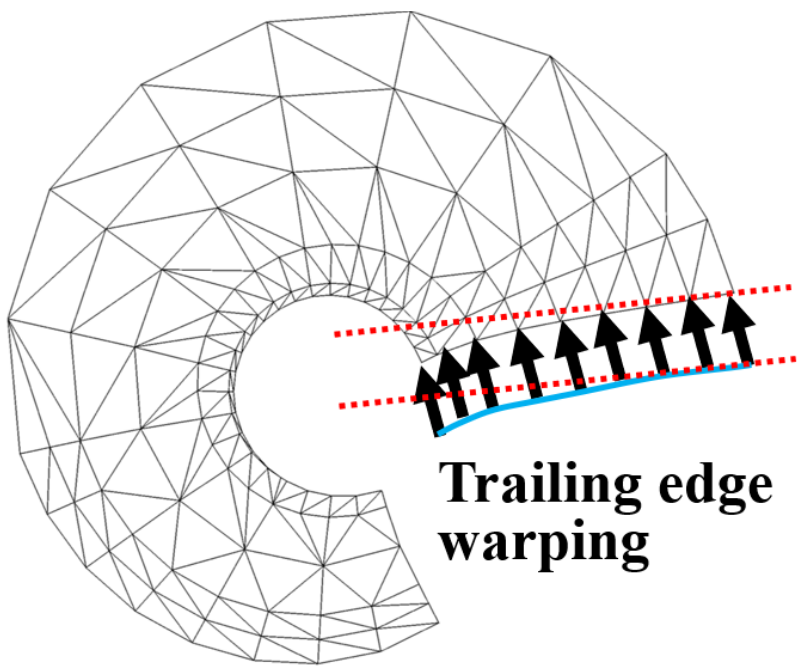

Figure 15: Flattened aerial screw surface material elements with curved leading and trailing edge.

To overcome this issue, material would be oversized to the least modified flattened pattern produced by SolidWorks software. To obtain 2D surface geometry, the aerial screw surface had internal elements compressed and extended in the software to retain internal and external length measurements needed to match those of the full 3D shape. The flattened surface is shown in Figure 15 to illustrate the non-standard shape deformation required to flatten an aerial screw surface. When converted to a flat surface, the inner radial sections were compressed, such that they needed to be stretched to fit the final 3D shape. The outer surface was also compressed, but at a lesser ratio to the inner surface, allowing it to be better fitting to the final 3D shape. The effect of this compression can be seen at the leading and trailing edges of the flattened surface where the edges reveal a non-linear shape, indicating element stretching and compression.

Chapter 5: Fabrication of 15.25 cm (6-in) Diameter Aerial Screws

Initial Physical Rotor Parameters

Construction of physical rotors is necessary for testing, analysis and comparison to computer models for verification. Models of aerial screws allow for identification of areas that require innovations and more focus that may be overlooked in software. Physical testing also helps to prove or disprove working theories of flight mechanisms such as the bound tip vortex. This section explores the fabrication considerations and steps taken to create a functional aerial screw vehicle.

Table 1 lists the geometric parameters used for each hand fabricated aerial screw. Of note in the initial fabrication is the lack of an uninterrupted upper surface, causing the spars to introduce turbulence and extra drag via the discontinuous surface. By having a non-smoothed upper surface, testing to confirm the existence of the bound tip vortex would be possible as discussed later. Each fabricated rotor shaft was machined from a template in order to reduce inconsistencies between rotors. Unfortunately, any imperfections found from the first shaft would be replicated on all subsequent shafts.

Table 1. Geometric parameters of first-generation physical aerial screw.

Parameter	Metric	English
Upper rotor radius	3.8 cm	1.5 in
Lower rotor radius	7.6 cm	3.0 in
Rotor taper ratio	1:2	1:2
Rotor number of turns	1.0	1.0
Rotor height	10.4 cm	4.1 in
Effective rotor area (all rotors)	729 cm^2	113 in^2
Distance between Adjacent rotors	18 cm	7.1 in
Upper tip speed	28.0 m/s	92 ft/s
Lower tip speed	55.9 m/s	184 ft/s
Number of Turns	1	1
Number of blades	2	2

Initial fabrication used 15.25cm (6in) long wooden shafts to allow for excess motor mating material to prevent physical interference between the blades and airframe. As designed, holes for 9 spars were positioned at 45° from each other and spaced vertically by 1.25cm (0.5in) to meet the desired pitch and number of turns. Each spar was cut to match the 2:1 taper:pitch ratio used for the best performing physical tests conducted by UMD graduate and undergraduate teams.[2]

Methods of Machining and Motor Mating

Fabrication of shafts and spars were straightforward as they both were cut to length using templates, while the shafts had spar holes drilled from a form fitting template. Skin material was also cut from oversized templates seen in Figure 16 in order to allow for self-adhesion. Oversizing also allowed for the surface to stretch into place on the 3D surface as mentioned earlier.

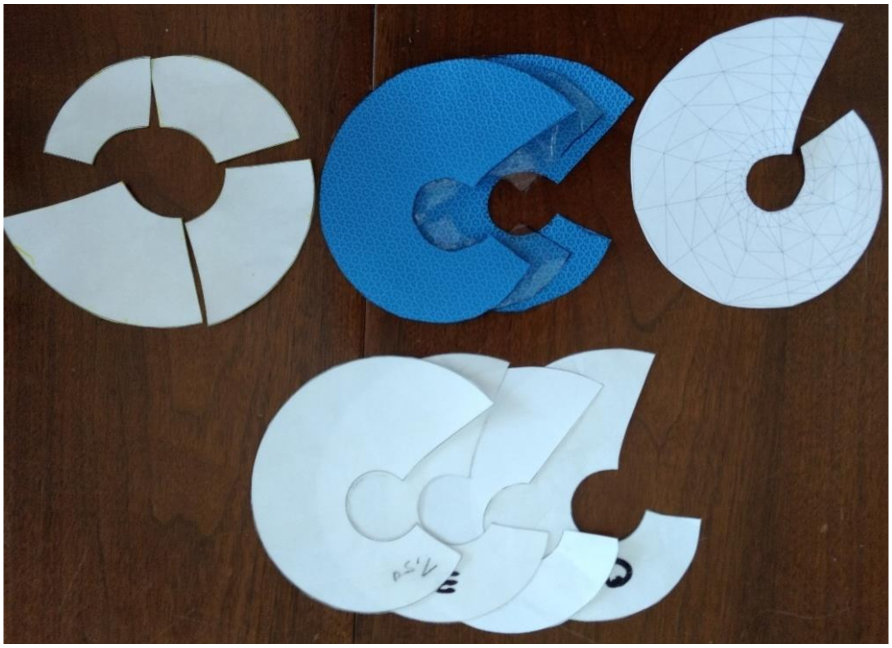

Figure 16: Oversized skin material templates for measuring mylar surface.

Connections to the motors were the next hurdle, as the shafts needed direct mating methods to transfer thrust, torque and any oscillating loads due to imbalanced rotors. Since each motor included a short, ~1cm threaded shaft, mating methods would attempt to leverage both the threads and shaft height to transfer torque and off-axis moments. The attempted mating methods seen in Figure 17 included Helicoil inserts, bronze threaded inserts, direct threading and additional 3D printed adapters. Bronze threaded inserts would require larger shaft diameters, leading to more mass, while Helicoil inserts could not mesh with the wood shaft without splitting the shaft. Thus, adapters were chosen as the most controllable and least destructive method.

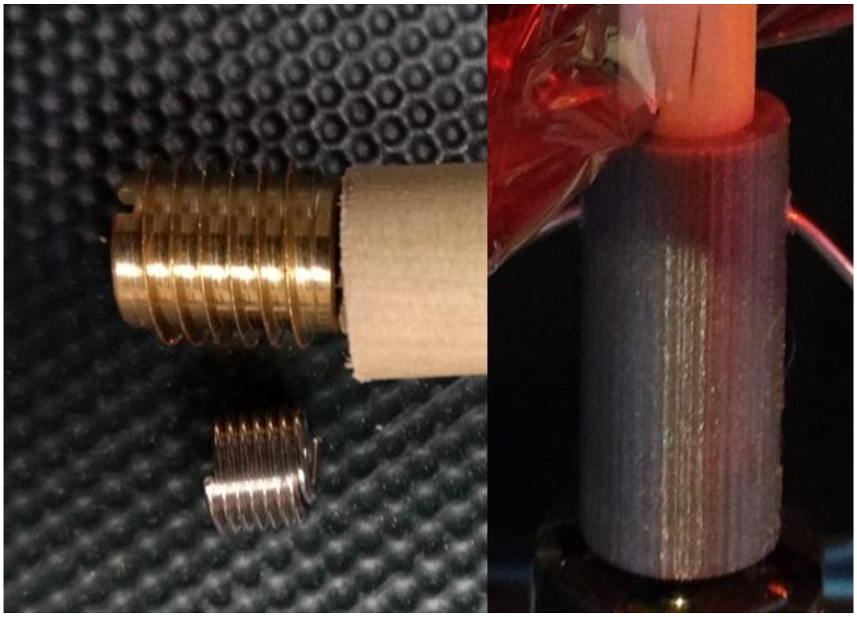

Figure 17: Attempted mating methods for aerial screw shafts. Helicoil and threaded inserts left, 3D printed adapter right.

The adapters were constructed of 3D printed PLA plastic and attached to the motor shafts via additional internal nuts. The total weight of all additional parts increasing the mass of each rotor by 1.33 times. The other mating methods provided much lighter options, but would provide a pathway for unplanned shaft failure due to small wall thickness and weak Young's modulus provided by the wood. Each of the internal methods would also be weak when responding to RPM changes or general torque requirements due to weak shear transfer between materials.

Adapters were not without faults of their own, including weight increase, torque transfer capability, shaft height increase and misalignment amplification. As such, it should be noted that rotors tested in this paper were not meant to be ideal iterations, but rather functional models. As such, fully fused deposition modeling 3D printed rotors were avoided due to their large increase in mass despite their fabrication consistency. The increased mass not only increased thrust requirements, but torque due to drag and moment of inertia. Less dense, structurally equivalent printing material may be explored to reduce inconsistency issues in future tests.

Table 2: Mass of each rotor part with different shafts.

Rotor Part	Metric	English
Shaft (wooden)	14.54g	0.513oz
Shaft (aluminum)	12.04g	0.425oz
Spars	3.83g	0.135oz
Surface material	5.67g	0.200oz
Steel tip wire	2.16g	0.076oz
Adapter (with nuts)	7.86g	0.271oz
Total (wooden)	34.06g	1.20oz
Total (aluminum)	23.70g	0.836oz

Initial Results of Early Fabrication

Testing of wooden shaft, adapter-held aerial screws revealed surprising trends into the performance of aerial screws. As mentioned earlier, the main lifting mechanism identified by CFD was the bound tip vortex which causes a low-pressure area above the tip of each blade. To test their formation without flow visualization, the upper surface was left as is in order to have spars exposed directly to the flow, potentially breaking up any tip vortex before it could develop fully. Testing of rotors in this configuration yielded thrust values between 65 and 80 grams (0.785N) per rotor. Considering the full vehicle mass was over 600 g, each rotor would need to produce more than twice their measured thrust. When comparing to traditional rotor blades seen in Figure 18, the aerial screws produced nearly 3 times less thrust for twice the power at 40W. Each traditional rotor produced up to 225 g at 15-20W, which highlights the first measured difference between aerial screws and traditional rotor blades.

Figure 18: “6x4.5” quadcopter rotor blades used for comparison to aerial screws.

Next, each aerial screw was modified to include a smooth upper surface, an addition of ~1.25g per rotor, to test the performance gain of a fully developed and uninterrupted tip vortex. Under ideal conditions of full power to a single rotor, the aerial screws were able to produce 150g of thrust each after adding the upper surface. Power draw remained similar to the previous testing case, yet the increase of thrust brought aerial screws closer to the performance of traditional rotors. Since the only variable changed between the two test cases was the addition of an upper surface, it can be inferred that a smooth fully formed continuous tip vortex supported by the upper surface was responsible for the increase in lift. The theory is further supported by other undergraduate flow visualization testing conducted at the University of

Maryland, which identified flow ingestion at the upper surface of each aerial screw indicating the presence of a low-pressure zone.

The testing also revealed several inherent weaknesses of the wooden rotor shaft fabrication methods. The most notable drawback of wooden rotor shafts was the warping of the shaft in differing atmospheric conditions causing rotor instability at high RPM. Additionally, the shafts were made artificially taller than planned due to needed mating surface area within the 3D printed adapters. Increased height provided a large moment arm for oscillations to take hold. By increasing the height, any force resulting from mass or lift imbalance would provide a larger moment to the adapter and motor, increasing power draw and reducing the maximum possible RPM. Utilizing the previously mentioned methods of attachment would not solve either issue, as each method would require additional support to fix structural problems while still having the problems associated with an environmentally susceptible shaft.

Updated Rotor Fabrication

To resolve most issues of material selection and fabrication consistency, the shaft type was changed to an aluminum tube. Previously wooden shafts were replaced with structurally equivalent metal shafts having greater mass, but metal allowed for tube shafts of lesser mass than the initial wooden shafts. Figure 19 shows the final iteration of hand-fabricated aerial screws for testing based on the aluminum shaft.

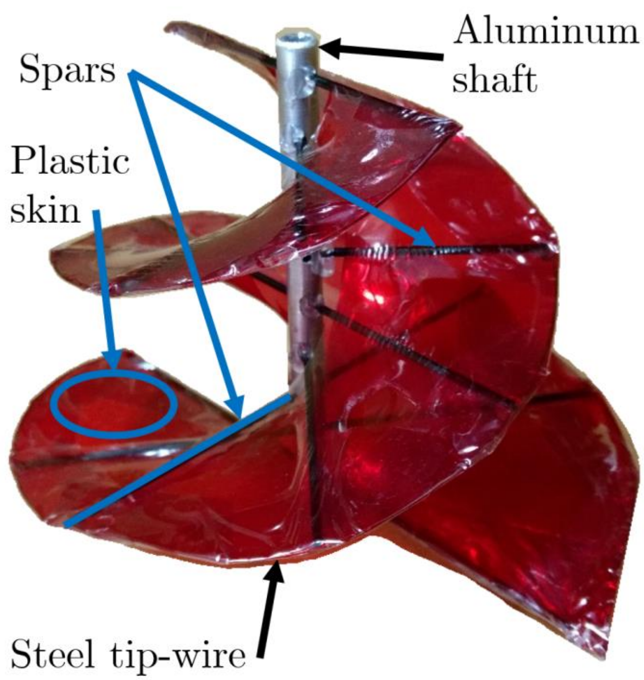

Figure 19: Current 2-bladed, single turn, novel Leonardo da Vinci aerial screw rotor.

The aluminum tube allowed for internal threading to mate directly to the existing externally threaded motor shafts. Not only would this reduce fabrication complexity, but would decrease rotor height, and inadvertently reduce weight of the rotors. Each aluminum shaft was found to be 12g, where each wooden shaft was 14.5g, with a 7.9g adapter assembly each. The change to aluminum shafts removed excess weight, reduced shaft misalignment issues and increased repeatability and durability of the design. The aluminum shafts used can be seen in Figure 20, where the spar hole locations are machined using precision milling machines and the internal threads cut on a manual lathe.

Figure 20: Aluminum shaft closeup of internal threads and exterior spar through-holes.

Every other aspect of the aerial screw design remained the same, including the skin surface, spar length and position, and steel tip wire. Of note is the difference in diameter for the shafts. The wooden shaft diameter was over 2 times larger than the newer aluminum shaft, but provided less than half of the stiffness. A side effect of the radial difference was the introduction of a larger gap between skin material and the central shaft. Air flow and lift nearing the shaft was shown to be inconsequential by Sutherland.[2] As such, no extra material, nor any additional consideration was focused toward making the inner sections of material conform to the central shaft of the aerial screw. Replacing the shafts with aluminum now allowed for testing to continue with less effort spent on balancing rotors to each other. As such, repeatable data collection and flight tests were then able to be executed.

Chapter 6: Testing a Functional Aerial Screw Vehicle

Stabilization of the Vehicle

To test the full quadcopter aerial screw vehicle, it needed to be stabilized for the unique flight characteristics of aerial screws. Due to their large distribution of mass, aerial screws have an increased vehicle and rotor moment of inertia when compared to traditional rotor blades. The fabricated aerial screws present an axial rotor moment of inertia of ~180gcm^2 while the traditional blades provide only ~110gcm^2. The increased rotor inertia lends itself to a more responsive yaw control while influencing pitch and roll control of the vehicle due to gyroscopic effects. Additionally, the newer aerial screws were tested to provide up to 300g of thrust in ideal conditions while drawing less than twice the power of traditional rotors, thus displaying an increase of thrust and efficiency.

Testing of aerial screws began with individually spinning up rotors which allowed for collection of thrust vs power, thrust vs RPM, FM vs RPM and C_T vs FM data seen in Figures 21 through 24. The single rotor testing allows for calculation of FM, PL (Power Loading) and DL (Disk Loading) among other performance metrics of rotorcraft. Each test of the isolated aerial screws brought throttle up to 90% maximum, as aerodynamic oscillations were introducing instabilities causing power measurement errors which overtook average power readings. However, thrust values for aerial screws at the throttle values above 90% were observed consistently over 300 g.

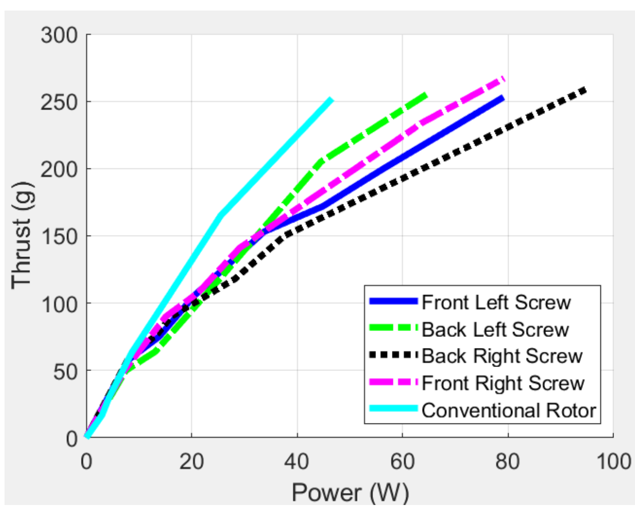

Figure 21: Plot of aerial screw and traditional rotor thrust as a function of electrical power.

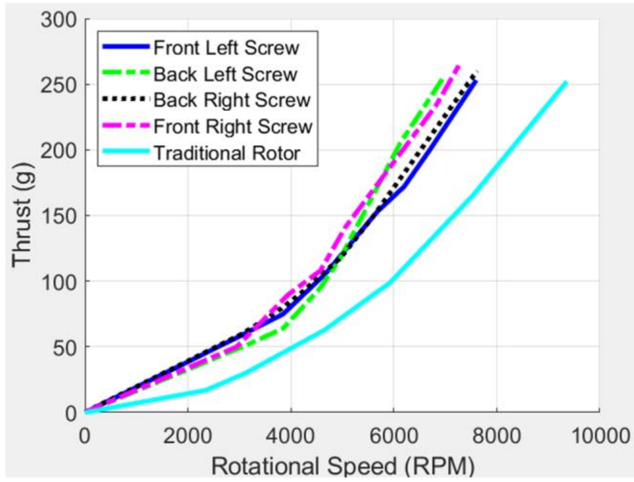

Figure 22: Plot of aerial screw and traditional rotor thrust as a function of RPM.

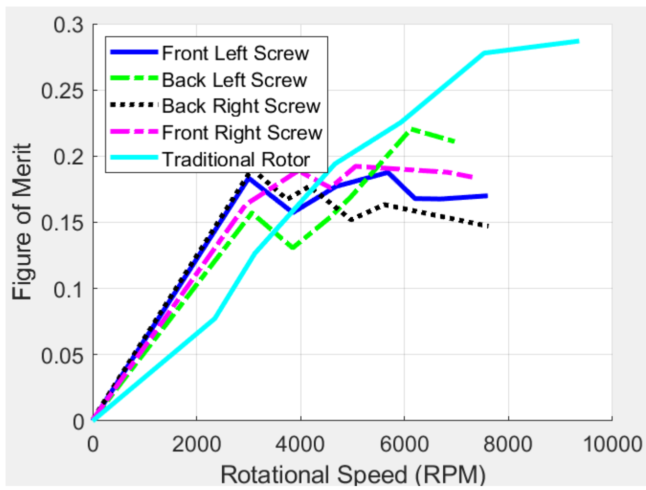

Figure 23: Plot of aerial screw and traditional rotor FM as a function of RPM.

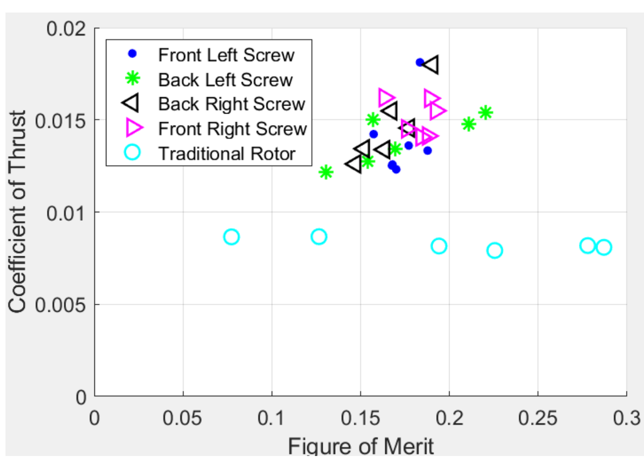

Figure 24: Plot of aerial screw and traditional rotor Coefficient of Thrust as a function of FM.

Of note is the relatively low FM compared to modern large-scale rotorcraft. Large vehicles will maintain a maximum FM around 0.7 while the small-scale tested in this paper produces a maximum FM of 0.225 because of reduced Reynolds numbers. Hrishikeshavan tested similar scaled traditional rotors with FM of similar value to the aerial screws tested here.[5] The effect of flying at a reduced Reynolds number region drops efficiency but still allows for functional testing and quantification of results. Individual rotor testing also allows for the revelation of aerial screws to have more aggressive curves, indicating aerial screws are more sensitive to RPM change inputs. Increased thrust at each RPM step is a product of increased power requirements for aerial screws resulting from larger surface area and profile drag.

Stabilization of the Vehicle

Before flight testing the completed vehicle, it must be stabilized in the pitch, roll and yaw axis. As mentioned earlier, yaw authority is increased due to the increased moment of inertia brought on by the heavier aerial screws. Similarly, roll and pitch require non-standard values in order to account for the increased inertias compared to traditional rotors. Gyroscopic precession may be ignored for small scale, but may play a larger roll with increasing scaled aerial screws, especially those in a single main rotor configuration.

To assist with stabilizing the vehicle while reducing destructive risk, a 3-axis gravity assisted gimbal stand was created. The full vehicle assembly was then mounted to the test stand such that the vehicle self-leveled to horizontal. The calculated center of gravity was only 0.5in below the pitch and roll pivot points, resulting in the stand not applying large stabilization forces to the system. When tuning system controls on a stand, the natural oscillation frequencies and mass must be considered so as to not misrepresent performance when off the stand. Perturbed oscillation tests revealed the first frequencies for pitch and roll to occur at 1.75 and 1.5 Hz respectively, both of which were well below any operating frequency of the rotorcraft. Higher frequencies may have been a result of structural properties and ground resonance, but performance on and off the stand revealed no difference. Additionally, any pitch and roll oscillations amplified by the control loop would result from 50 Hz or higher ranges, ignoring the test stand frequencies.

Control Scheme

The control scheme used for the quadcopter configuration was that of a tuned PID loop fed from gyroscope rate readings. Tunable parameters included all three gains (proportional, integral, derivative), gyroscope filters and D-gain filters. Stabilizing the aerial screw quadcopter can be broken down into two stages: the stabilization of pitch and roll motion and the removal of excess noise overpowering filters and gains.

Filtering of gyroscope and D-gain noise was accomplished using multiple standard lowpass filters in conjunction with notch filters. The most prevalent noise introduced to the system was 1/rev oscillations from the aerial screws. Despite refined fabrication and machining methods, the aerial screws retained imperfect shaft alignment and surface application. Small misalignments noted at the base were amplified to create larger offsets in the upper portions of an aerial screw. These oscillations were more likely caused by aerodynamic imbalance than mass imbalance or offset. According to current testing and testing conducted by the UMD graduate design team, the aerodynamic loads provided by the aerial screw surface cause larger reactionary moments about the shaft base than mass offsets at high RPM.[2] The moment generated by aerodynamic forces of a singular blade on an aerial screw is found as 3.3Nmm (0.024 lbft), while the largest expected mass offset moment induced from rotation is 0.6Nmm (0.004 lbft). When spinning a rotor at low RPM the rotor follows any shaft offset (misalignment), but at RPM ranges below that necessary for takeoff yet enough to generate ~50% maximum thrust, the aerodynamic loads and gyroscopic precession stabilize the aerial screws such that they oscillate at a lower magnitude. At and above operating RPM, the aerodynamic imbalances from imperfect fabrication overtake any gyroscopic effects and induce 1/rev oscillations to the system which then need to be filtered out.

As mentioned, a notch filter was used to reduce the effect of 1/rev oscillations, but it was only tuned to the hover RPM frequency. To account for higher frequencies overtaking D-gain, a low-pass filter was used in conjunction with the notch filter, reducing frequencies higher than operational speed, which would be induced from rotor interaction or circuit noise. A side effect of such aggressive filtering is a slower response time to rapid maneuvers and potential aliasing of important high frequency feedback of input commands. It should be noted that a slower response in flight testing can be qualified as a “slightly sluggish response to stick inputs” and is not a detrimental performance loss.

A Ziegler-Nichols tuning scheme was used as a baseline in trying to determine operational PID values for the aerial screw vehicle while manual tuning determined final gain values. The basis of the Z-N tuning scheme is derived from the primary oscillation frequency at first system instability. By first setting both integral and derivative gains to 0, the proportional gain can be increased until the onset of oscillation. Then, using the frequency at which the system oscillates ($T_{ultimate}$) and the P-gain value ($K_{ultimate}$), the I-gain and D-gain can be determined using the following equations:

$$K_i = \frac{1.2K_u}{T_u} \quad and \quad K_d = 0.75K_uT_u$$

To resolve the P-gain, it is set between 0.4 and 0.6 times the value of onset of oscillation. More aggressive tuning lowers the value to create a system which reduces overshoot, but also reduces response time. In an experimental unstable aircraft such as the aerial screw quadcopter, stability is prioritized over response time, as a more stable vehicle produces more repeatable data and results.

Final tuning of PID gains was achieved by manual adjustment to allow for piloted flight rather than autonomous flight. Although autonomous flight would provide more consistency between tests, the extra mass from on-board hardware combined with excessive filtering make the current vehicle a poor choice for autonomous flight systems. Gains were tuned on the gimballed test stand, thus providing a pathway for future stabilization issue resolution, however the gains were under tuned on the test stand to allow for manual flight.

Flight Testing

Unrestrained flight testing allows for data collection of different flight scenarios including hover and forward flight. The initial tests were conducted in hover to determine efficiency and to prove stability of the vehicle. Subsequent tests would delve into higher advance ratios in forward flight, where the advance ratio of an aerial screw was defined as the tip speed at the largest radial section divided by the Mach number at time-of-test air conditions. Flight test data collected includes RPM, power, humidity, position, pressure, temperature, elevation and velocity. The values can be extrapolated to determine efficiency in the form of FM and effects such as power reduction in forward flight, etc.

Power data is collected from on-board voltage and current sensors recording overall vehicle power consumption as mechanical measurement methods would increase mass of the vehicle further. As such, actual performance values of rotors tested in this report are based on electrical power readings. Larger scale testing may opt to include mechanical methods of shaft power measurement to better capture power requirements of aerial screws. In earlier rotor testing, each rotor was throttled up by itself, reducing error from other rotors; however, during flight testing, power of all rotors is combined into a single value that is shared with all other electronics of the quadcopter. Thus, the value of power consumed for each rotor presented in this paper is above ideal, meaning actual performance and efficiency are better than presented.

Hover

Hover testing is used to determine a baseline power consumption and performance before attempting forward flight. It also allows for additional fine tuning of PID gains prior to collecting data in differing forward flight conditions. Without constant PID values, motor performance may be influenced by noisy signals and unplanned maneuvers, affecting measured values of power and RPM.
Hover performance of traditional rotors and aerial screws can be seen in Figure 25 where the aerial screws are shown to have nearly double the power requirements of a conventional rotor. Recalling the difference in operating RPM at any given thrust, where aerial screws spin at lower speeds than traditional rotors to generate a similar thrust, again supporting the finding of aerial screws to be more sensitive to RPM changes.

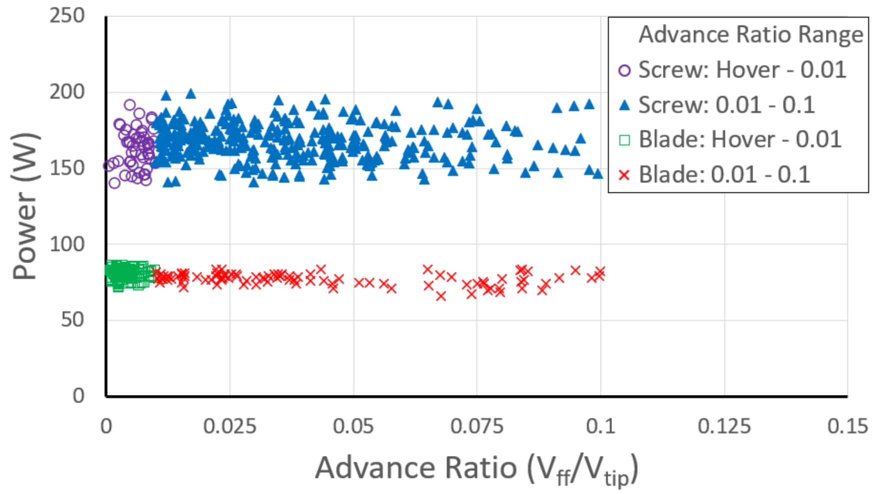

Figure 25: Performance test values of aerial screws and traditional rotors.

Table 3: Aerial screw and traditional rotor generalized rotor performance.

	FM	DL (lb/ft^2)	PL (lb/hp)
Wooden screw	0.0419	0.954	2.237
Aerial screw 1	0.1701	2.842	5.260
Aerial screw 2	0.2110	2.846	6.502
Aerial screw 3	0.1643	2.920	5.013
Aerial screw 4	0.1841	2.999	5.544
Traditional rotor	0.2507	2.527	8.223

From hover and test stand data, the FM, DL and PL values for each aerial screw and traditional rotors were collected and are listed in Table 3. Wooden shaft aerial screws are also included in the table to illustrate the performance increase gained by changing shaft material and motor mating method. FM is important to the quantification of aerial screws as a viable VTOL metric since FM can be used to place aerial screws relative to other forms of VTOL vehicles. Figure 26 shows a plot from Leishman of different VTOL vehicles and their power and disk loading values.[4] Aerial screws are included as a range due to the variance in small scale testing and as such, are noted by the shaded oval.

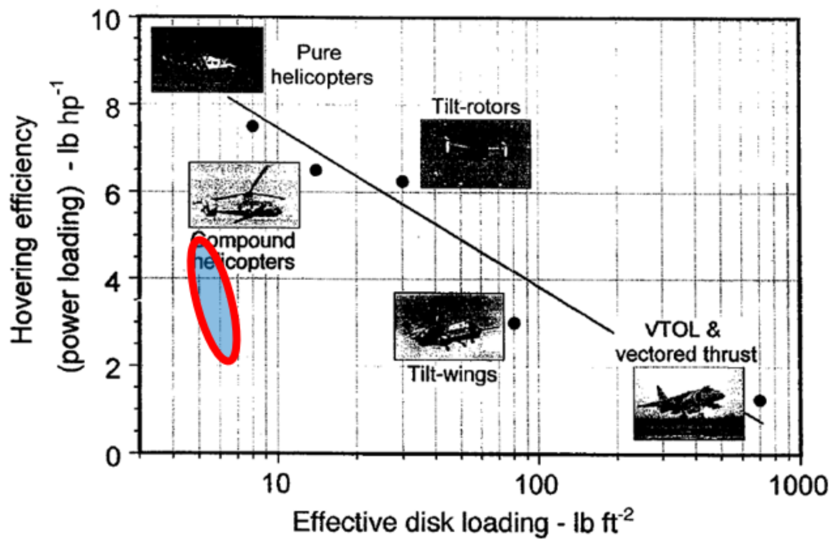

Figure 26: Plot of different VTOL vehicle configuration's power loading vs. disk loading.

Aerial screw performance on the plot shows a general trend of underperforming, however the scale at which testing occurs must be considered. Hrishikeshavan conducted tests of multiple size shrouded and unshrouded rotors for small scale rotorcraft to identify performance in low Reynolds number flight regimes.[5] Since the aerial screws operate in low Reynolds number regions, comparisons can be made using Hrishikeshavan's experiments. The plot in Figure 27 provides a better relative comparison to other similarly sized VTOL vehicles. Aerial screws can again be placed on the plot; now with the performance being comparable to other traditional rotors of similar size. The aerial screws still are slightly underperforming compared to the conventional rotors, but they have clear paths for improvement. Better fabricated, larger aerial screws would perform similar to or better than low disk loading VTOL vehicles due to their large solidity profile and hover efficiency. Although, as all VTOL vehicles increase hover efficiency, their forward flight performance suffers due to lack of edgewise flow optimizations.

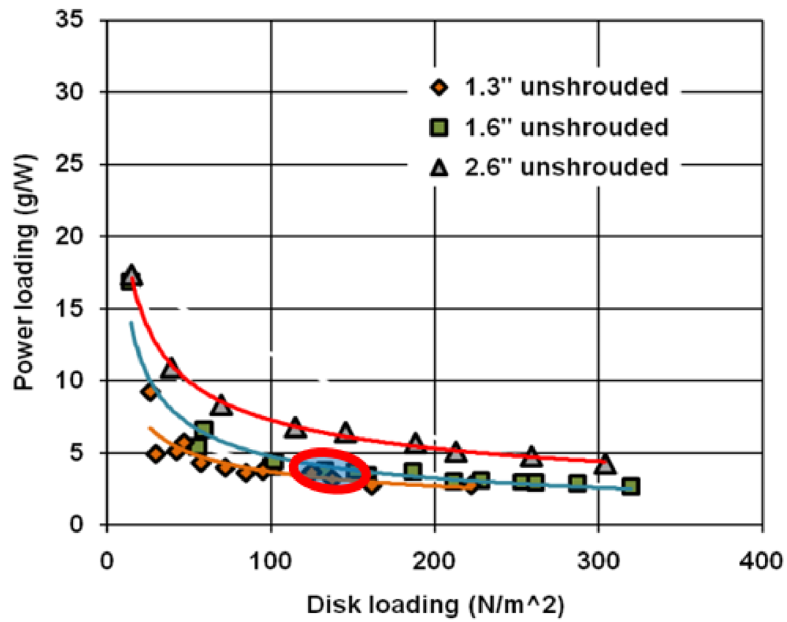

Figure 27: Plot of different mini-VTOL vehicle configuration's power loading vs. disk loading.

Forward Flight

Forward flight presents multiple interesting developments for aerial screws. Not only does an aerial screw have increased mass compared to traditional rotors, but it has a large flat-plate area and large induced and profile drags. Both of those aspects account for the increased power requirements mentioned earlier. Figure 28 shows the performance of traditional rotors tested in forward flight while Figure 29 shows aerial screws tested on the same frame/hardware in forward flight.

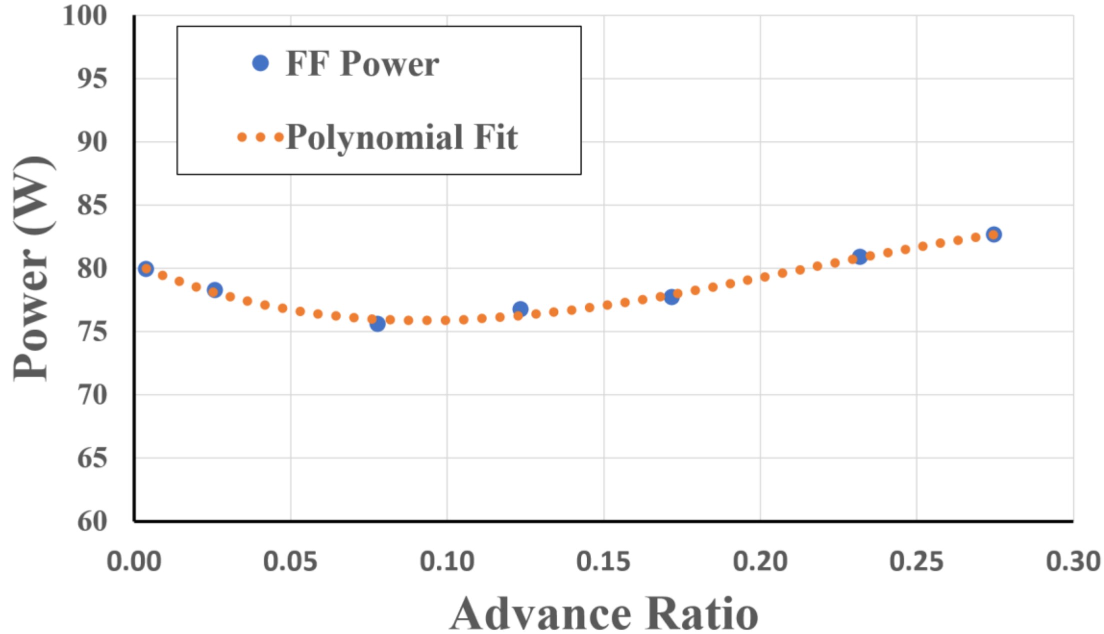

Figure 28: Traditional rotor forward flight power curve using frame and hardware of aerial screw vehicle.

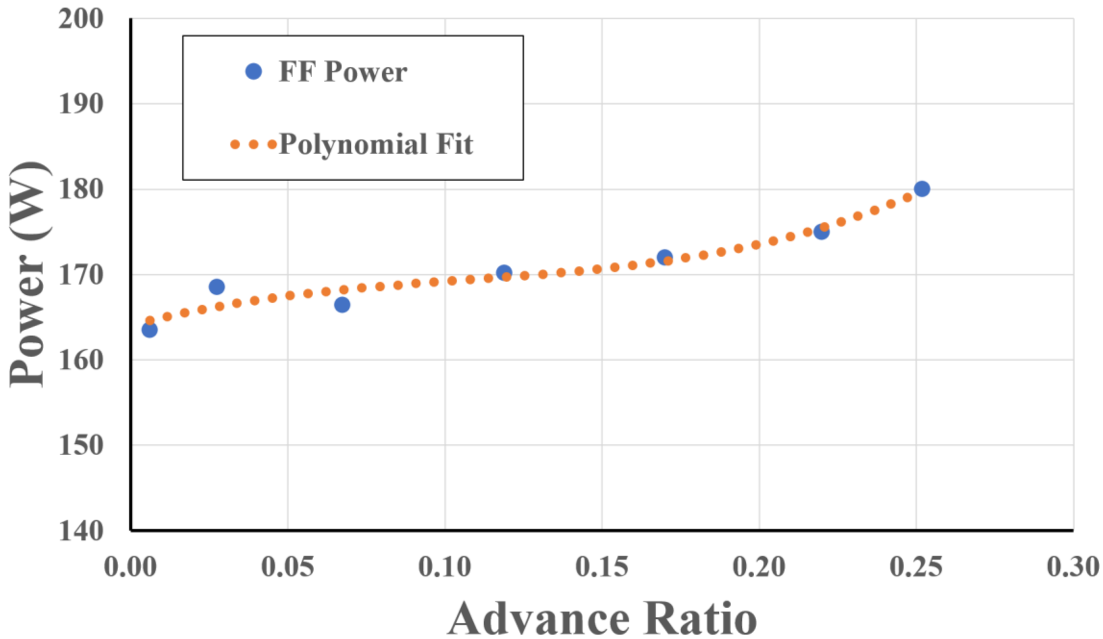

Figure 29: Aerial screw forward flight power curve.

As expected, the traditional rotors encounter reduced power requirements as advance ratio increases to ~0.1. Then power increases with further increasing advance ratio as expected. Aerial screws show a differing trend of increasing power requirements as advance ratio increases. At a similar advance ratio where traditional rotors have reduced power, aerial screws instead trend to plateau power temporarily before continuing to increase. The exact rate at which this occurs is not clear, but should be explored further if attempting to quantify aerial screw forward flight performance in more detail. Data for high-speed forward flight aerial screw performance is not available as the vehicle is mechanically difficult to control at constant speeds at high advance ratios. Forward flight speeds exceeding 5m/s (16ft/s), an advance ratio of >0.1, are not easily maintained and thus have a reduced amount of data points when compared to <0.1 advance ratio tests. Further testing at higher forward flight speeds is required to fully characterize the performance of aerial screws.

Testing forward flight also allows for a qualitative analysis of flight characteristics. Due to the increased rotor inertia, throttle changes and pitch and roll adjustments are less instant than with traditional rotors. The increased inertia plays into yaw efficacy unlike roll and pitch in a quadcopter configuration due to yaw control being actuated by differing torque through RPM changes. If in a single main rotor configuration, the anti-torque required from an aerial screw would be greater than a traditional rotor, requiring more power to be diverted towards the tail.

Preliminary climb and descent testing revealed qualitative results regarding aerial screw performance. When in descent, aerial screws utilizing tip vortex lift are prone to detrimental propwash interactions reducing thrust and causing instability. The propwash interactions occur at lower descent rates than traditional rotors due to the decreased downwash velocity of aerial screws. At greater descent rates, the aerial screw is able to function normally. Climb conditions follow similar trends for those of traditional rotors. Aerial screws utilizing volume displacement thrust (ducted) may be less prone to propwash interactions seen with tip vortex testing.

Chapter 7: Discussion of Results

Discussion

Aerial screws of a small scale are shown to function similarly to rotor blades in an identical environment, disproving a long-standing belief that aerial screws were incapable of flight. The aerial screw is able to leverage a mechanism of flight unique to delta-wing aircraft and aerial screws in order to obtain sufficient thrust for hover and forward flight. By identifying and proving the function of the bound tip vortex, it is possible to consider optimizing the geometry of an aerial screw to leverage maximum thrust, hover efficiency, or forward flight characteristics. If an aerial screw were to be designed for hover efficiency with variable taper, pitch, anhedral, etc. it may surpass calculated values of FM for conventional rotors in the subsonic flight regime. It may be found that an aggressive pitch and taper variation that follows downwash patterns of regular rotorcraft provides more thrust than a constant pitch, constant taper surface.

As mentioned earlier, flow visualization testing has shown aerial screws to have considerable radial ingestion of air, further solidifying their role as a low advance ratio rotor.

Future Considerations

A common source of error for every rotor tested in this paper is the oscillation present due to imperfect machining and fabrication techniques. Slight mass imbalances impact low RPM performance, while geometry imbalance between two blades of the same rotor causes aerodynamic loads to be imbalanced at high RPM. When encountering imbalances and oscillations, the motors must be supplied more power to sustain constant thrust/RPM. Thus, efficiency is artificially reduced unlike most modern rotorcraft blades. If aerial screws are to continue development, special care should be taken to plan and fabricate identical blades on a single rotor and rotors nearly identical to each other.

Some fabrication processes that may aid in reducing error include 3D printed rotors, custom carbon fiber blade molds and CNC shaft machining processes to name a few. By planning for repeatable and consistent rotor fabrication, blade balancing will require less effort between rotors, allowing for increased efficiency and better control authority/performance overall.

An additional area of interest is the formation and sustainability of the bound tip vortex during flight maneuvers. In forward flight, as a section of blade passes the forward section of the rotorcraft, it will experience additional radial ingestion, potentially moving the tip vortex radially inward. While the aft portion of blade may not experience enough ingestion or be experiencing interference from upper sections of the same rotor. Due to their nature of including continuously wound large solidity blades, aerial screws may experience additional areas of low lift similar to reverse flow regions on traditional blades.

Conclusions

1. The 600 g quadcopter relied on four 6-in diameter aerial screws as a main source of propulsion and control, demonstrating a functional proof of concept. By spinning at 7000 to 8000 RPM, aerial screws of this size were capable of generating >300 g of thrust each, more than 1.25 times that of equivalently sized traditional rotors.
2. Aerial screws are proven as capable VTOL lifting surfaces with unique aerodynamic mechanisms capable of supporting scaling to larger sizes including but not limited to human carrying scales. Both large volume displacement and bound tip vortex methods of lift via aerial screw provide significant thrust for the power delivered.
3. The bound tip vortex for aerial screws provides significant (80%) thrust for the geometry utilized, indicating a need for continuous upper surfaces when

utilizing the tip vortex thrust method. By tailoring geometry to aid the tip vortex, hover performance can be increased further.

4. When comparing disk loading and power loading of aerial screws with other VTOL vehicles, it is evident that with slight improvements in fabrication, aerial screws can easily be competitive with conventional helicopter rotors in hover efficiency.
5. Flight controls for aerial screws have increased control authority in yaw maneuvers while reducing responsiveness slightly in pitch and roll maneuvers due to the larger moment of inertia and mass compared to traditional rotors. Other configurations require consideration of gyroscopic effects from the increased rotor inertia.
6. The vortex ring state is attained at lower descent velocities compared to traditional rotors due to the lower downwash velocity present with aerial screws. Descent should be explored further to determine the range at which the vortex ring state is present, resulting in safe operation ranges.
7. Aerial screws require further investigation to optimize geometry for efficiency just as traditional rotor blades have. Upon optimizing aerial screw geometry, they have the capability to rival or surpass traditional rotors in thrust, control authority and hover efficiency.

Bibliography

1. Lambermont, P., Pirie, A., *Helicopters and Autogyros of the World*, Cassell, London, 1970, Chapter 2.

2. Sutherland, J., Brown, R., Ebewele, E. Fisler, E., Krohmaly, K., Linkins, J., Marepally, K., Prete, A., Semenov, I., Nagaraj, V., Chopra, I., Datta, A., "Leonardo's Aerial Screw: 500 Years Later", University of Maryland, 2020.

3. Polhamus, Edward C., "A Concept of the Vortex Lift of Sharp-Edge Delta Wings Based on a Leading-Edge-Suction Analogy", NASA TN, Langley Research Center, 1966

4. Leishman, G. J., *Principles of Helicopter Aerodynamics*, Cambridge University Press, New York, NY, 2006, pp. 65 & 145-149

5. Hrishikeshavan, V., Black, J., Chopra, I., Design and testing of a Quad Shrouded Rotor Micro Air Vehicle in Hover, 53rd AIAA/ASME/ASCE /AHS/ASC Structures, Structural Dynamics and Materials Conference 20th, Honolulu, Hawaii, April 23-26, 2012.